

Article

Toward Structurally Novel and Metabolically Stable HIV-1 Capsid-Targeting Small Molecules

Sanjeev Kumar V. Vernekar ^{1,†}, Rajkumar Lalji Sahani ^{1,†} , Mary C. Casey ², Jayakanth Kankanala ¹, Lei Wang ¹, Karen A. Kirby ³, Haijuan Du ³, Huanchun Zhang ³, Philip R. Tedbury ³ , Jiashu Xie ¹, Stefan G. Sarafianos ³ and Zhengqiang Wang ^{1,*} 

¹ Center for Drug Design, College of Pharmacy, University of Minnesota, Minneapolis, MN 55455, USA; vvsanjeev99@googlemail.com (S.K.V.V.); rsahani@umn.edu (R.L.S.); kankanalajk1@gmail.com (J.K.); leiwang@dlut.edu.cn (L.W.); jxie@umn.edu (J.X.)

² Department of Molecular Microbiology and Immunology, University of Missouri School of Medicine, Christopher S. Bond Life Sciences Center, Columbia, MO 65211, USA; mcc6x2@mail.missouri.edu

³ Laboratory of Biochemical Pharmacology, Department of Pediatrics, Emory University School of Medicine, Atlanta, GA 30322, USA; karen.kirby@emory.edu (K.A.K.); haijuan.du@emory.edu (H.D.); huanchun.zhang@emory.edu (H.Z.); philip.tedbury@emory.edu (P.R.T.); stefanos.sarafianos@emory.edu (S.G.S.)

* Correspondence: wangx472@umn.edu; Tel.: +1-612-626-7025

† These authors contributed equally.

Received: 30 March 2020; Accepted: 14 April 2020; Published: 16 April 2020



Abstract: HIV-1 capsid protein (CA) plays an important role in many steps of viral replication and represents an appealing antiviral target. Several CA-targeting small molecules of various chemotypes have been studied, but the peptidomimetic PF74 has drawn particular interest due to its potent antiviral activity, well-characterized binding mode, and unique mechanism of action. Importantly, PF74 competes against important host factors for binding, conferring highly desirable antiviral phenotypes. However, further development of PF74 is hindered by its prohibitively poor metabolic stability, which necessitates the search for structurally novel and metabolically stable chemotypes. We have conducted a pharmacophore-based shape similarity search for compounds mimicking PF74. We report herein the analog synthesis and structure-activity relationship (SAR) of two hits from the search, and a third hit designed via molecular hybridization. All analogs were characterized for their effect on CA hexamer stability, antiviral activity, and cytotoxicity. These assays identified three active compounds that moderately stabilize CA hexamer and inhibit HIV-1. The most potent analog (**10**) inhibited HIV-1 comparably to PF74 but demonstrated drastically improved metabolic stability in liver microsomes (31 min vs. 0.7 min $t_{1/2}$). Collectively, the current studies identified a structurally novel and metabolically stable PF74-like chemotype for targeting HIV-1 CA.

Keywords: HIV-1; capsid-targeting antivirals; PF74; metabolic stability

1. Introduction

Human immunodeficiency virus 1 (HIV-1) encodes a Gag polyprotein which contains multiple protein domains for viral assembly and release: matrix (p17 MA), capsid (p24 CA), nucleocapsid (p7 NC), p6 and spacer peptides Sp1 and Sp2 [1]. Gag polyproteins assemble to form the immature viral capsid core, which upon protease cleavage rearranges into a fullerene-shaped mature capsid core [2] comprising approximately 250 CA hexamers and exactly 12 asymmetrically-distributed CA pentamers [3]. CA plays essential roles in viral assembly and multiple events during viral replication [4,5]. CA-CA interactions drive the assembly and disassembly of viral capsid, and capsid core stability is important for reverse transcription, nuclear entry, and cloaking of the viral DNA product from host nucleic acid sensing

mechanisms in the cytosol [6]. CA interacts with many cellular factors [7,8], including TRIM5 α [9,10], cleavage and polyadenylation specific factor 6 (CPSF6) [11,12] nucleoporins 153 [13–15] and 358 [16–18] (NUP153, NUP358), MxB [19,20], and Cyclophilin A (CypA) [21–23]. These interactions enable early viral replication steps, including uncoating, cytoplasmic trafficking, reverse transcription, nuclear transport, site of integration, and the evasion of innate immunity [24]. Hence, CA-targeting small molecules could confer both early and late stage antiviral phenotypes by perturbing the stability of viral capsid core and interfering with important CA-host interactions.

The CA structure [25–27] is mostly helical (Figure 1A): it comprises 7 helices at the N-terminal domain (CA_{NTD}) and 4 helices at the C-terminal domain (CA_{CTD}). Interactions between one CA_{NTD} and the CA_{NTD} and CA_{CTD} of an adjacent monomer form the molecular basis of stable hexameric lattice and virus-host interactions. Previous structural studies with CA-bound compounds have revealed a small molecule binding sites [28], such as the particularly interesting PF74 binding pocket. This pocket is formed primarily by H3 and H4 of the CA_{NTD} (cyan), and the H8 and H9 of the CA_{CTD} of an adjacent monomer (green) (Figure 1A). In addition to accommodating the binding [25,29,30] of PF74 and BI-2, a smaller CA-targeting molecule (Figure 1B), the same pocket is also used by important cellular factors, including [29,30]: Nup153, a nucleoporin important for nuclear transport of viral preintegration complexes (PICs); and CPSF6 which transports HIV-1 PICs to transcriptionally active chromatin [31]. PF74 is a well-characterized [32] peptidomimetic built around a phenylalanine core, and capped with an aniline moiety at the carboxylate end and an indole-3-acetic acid at the amino end (Figure 1B). All three components, the core, the aniline moiety (right) and the indole acid moiety (left), provide key molecular interactions for the binding of PF74 [25]. Consistent with the binding site and mode, PF74 displayed a concentration-dependent bimodal mechanism [32,33] of action: at lower concentrations it competes against host factors including CPSF6 and NUP153 to affect nuclear entry; and at higher concentrations it blocks uncoating and reverse transcription, presumably by altering inter-hexamer interactions [25].

Despite the attractive antiviral profile and the unique bimodal mechanism of action, PF74 is not a viable drug candidate due primarily to its prohibitively poor metabolic stability [34]. In human liver microsomes (HLMs), the half-life ($t_{1/2}$) of PF74 was less than 1 min [35,36]. This major deficiency strongly necessitates targeted efforts to search for structurally novel and metabolically stable small molecules capable of binding to the PF74 binding pocket. Along this line, the Zhan and Liu group recently reported PF74-like compounds where an easier and synthetically more accessible 1,2,3-triazole ring was substituted for the indole moiety [35,36]. However, such compounds were considerably (>10-fold) less potent than PF74 in antiviral assays and were essentially as unstable in HLMs [35,36]. Our current work features a pharmacophore-based shape similarity search approach based on PF74 (Figure 2A). Molecular similarity [37,38] is an important concept in medicinal chemistry and drug discovery. Hit generation using similarity search is based on the premise that similar chemical structure confers similar biological activity. In our search, we extracted the 3D conformation of PF74 from reported co-crystal structure (PDB: 4XFZ [25]) and defined 7 pharmacophore points (Figure 2A) according to its mode of binding, including two H-bond donors (D1 and D2), two H-bond acceptors (A1 and A2), as well as three hydrophobic moieties (H1, H2 and H3). This 3D pharmacophore was then used to screen against a subset of the ZINC database [39] (100K compounds) using the program PHASE [40,41]. Hit ranking was based on the number of pharmacophore points satisfied and the lead like properties as predicted by the Lipinski's rule of 5 [42]. From this similarity search we selected two hits (2 and 22) for analog synthesis and SAR (Figure 2B). Molecular hybridization [43] between hit 2 and PF74 also generated hit 11, which was also subjected to analog synthesis (Figure 2B). We report herein the analog synthesis and SAR on all three hits. In the end, our best compound inhibited HIV-1 with an EC₅₀ of 1.6 μ M, and more important exhibited a half-life ($t_{1/2}$) 44-fold longer than PF74.

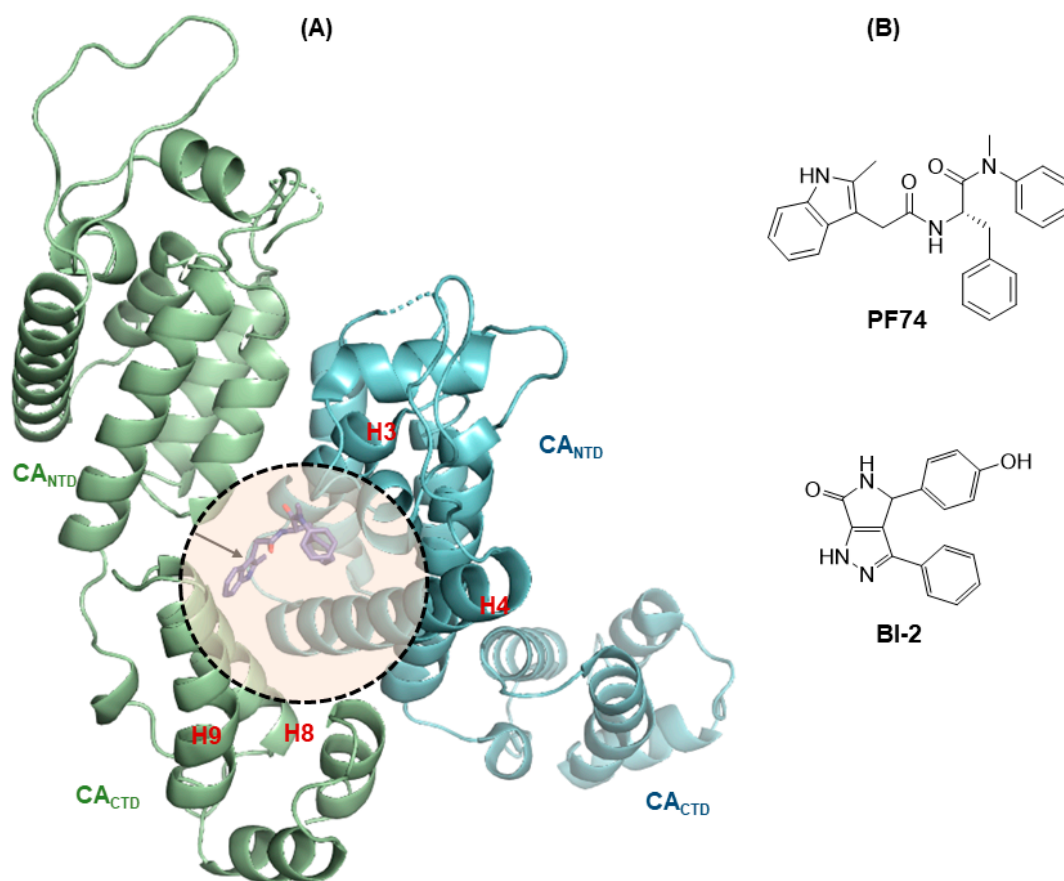
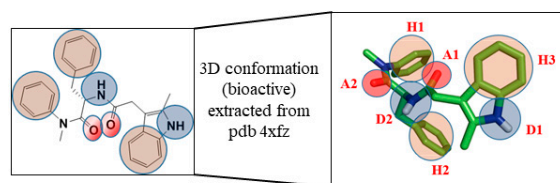


Figure 1. Structure of HIV-1 capsid protein (CA) and a key CA ligand binding pocket. (A) The structure of CA dimer (Protein Data Bank code: 4XFZ [25]). The pocket formed around H3 and H4 of the CA_{NTD} (cyan), and H8 and H9 of the adjacent CA_{CTD} (green) accommodates the binding of multiple ligands, including host factors Nup153 and CPSF6, and small molecules **PF74** and **BI-2**. Shown in the pocket is **PF74** (pointed to with an arrow); (B) chemical structures of **PF74** and **BI-2**.

(A) Pharmacophore & shape similarity search



D- H-Bond Donor (D1-2)
A- H-bond Acceptor (A1-2)
H- Hydrophobic (H1-3)

PHASE ↓ 100K compounds (subset of Zinc database)

Hits: 2 and 22 selected

Sorted based on:

- 1) Satisfying > 3 pharmacophore points (out of 7)
- 2) Lead like compounds (Lipinski's rule of 5)

(B) Hits and SAR

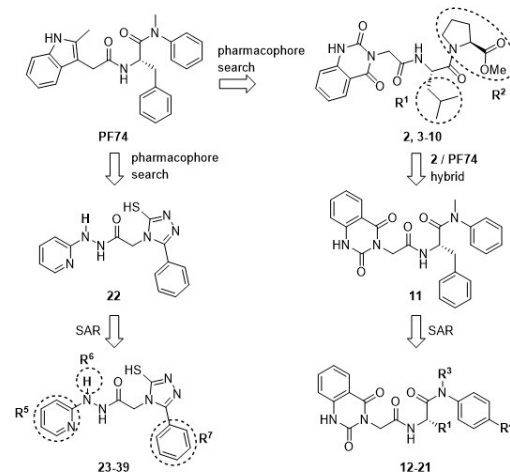
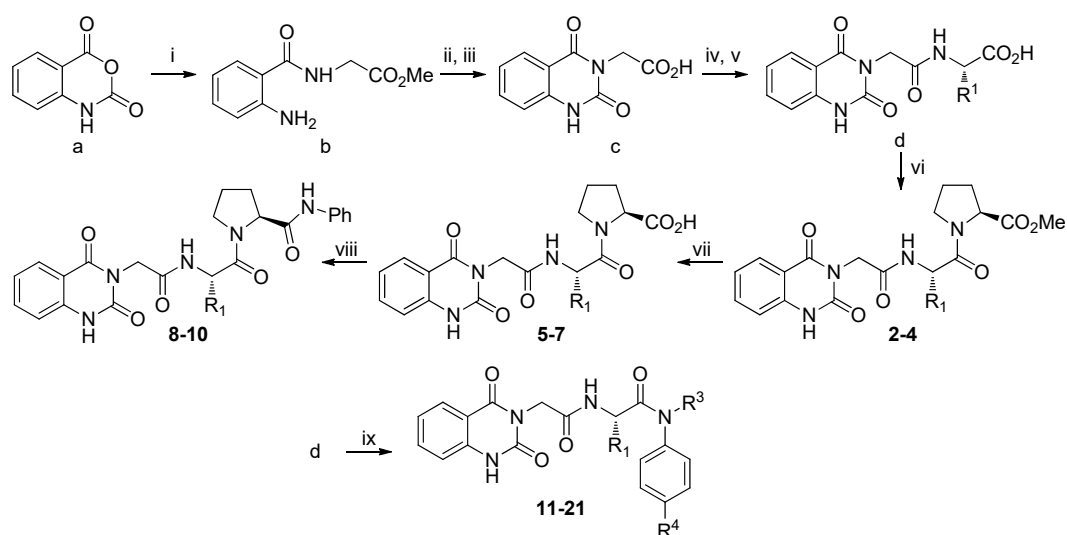


Figure 2. Generation of novel compounds targeting the **PF74** binding pocket. (A) Initial hits generated via a pharmacophore and shape similarity search; (B) SAR of two selected hits (**2** and **22**), as well as a new hit (**11**) from the hybridization between **2** and **PF74**. Compounds **3–10** are variants of **2**, with modifications in the circled regions.

2. Materials and Methods

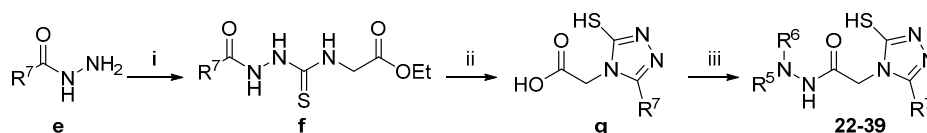
All analogs were synthesized using procedures described in Schemes 1 and 2, fully characterized with ^1H NMR, ^{13}C NMR, and HRMS, and displayed a purity of $\geq 95\%$ as determined by HPLC. Detailed synthetic procedures and compound characterization data are included in Supplemental Materials.

The general synthetic strategy for major analogs (1–39) tested in this work is described here (Schemes 1 and 2) and the synthesis for others is outlined in supporting information (Schemes S1 and S2). Commercially available 1*H*-benzo[*d*] [1,3] oxazine-2,4-dione (**a**) was reacted with glycine methyl ester hydrochloride in the presence of Et_3N in DMF to yield intermediate (**b**). Further treatment of intermediate (**b**) with ethyl chloroformate in pyridine and then with NaOH in MeOH/ H_2O afforded the carboxylic acid intermediate (**c**). A subsequent amide coupling of carboxylic acid intermediate (**c**) with different *L*-amino acid methyl ester hydrochlorides in the presence of HATU and DIPEA in DMF furnished acid intermediates (**d**) after hydrolysis under LiOH in MeOH/ H_2O . To synthesize varied hit 2 analogs, carboxylic acid intermediates (**d**) were further coupled with *L*-proline methyl ester hydrochloride in the presence of PyAOP and DIPEA to produce compounds 2–4, which upon hydrolysis afforded 5–7. Another coupling with various amines delivered analogs 8–10. Likewise, acid intermediates (**d**) were treated with various anilines using HATU and DIPEA in DMF to produce hit 11 analogs 11–21.



Scheme 1. Synthetic Strategy for Analogs 2–21. Reagents and conditions: (i) glycine methyl ester hydrochloride, Et_3N , DMF, rt, 12 h; (ii) ethyl chloroformate, pyridine, rt, 12 h; (iii) NaOH, MeOH/ H_2O , 60 °C, 12 h; (iv) *L*-amino acid methyl ester hydrochloride, HATU, DIPEA, DMF, rt, 12 h; (v) LiOH, MeOH/ H_2O , rt, 12 h; (vi) *L*-proline methyl ester hydrochloride, PyAOP, DIPEA, DMF, rt, 12 h; (vii) LiOH, MeOH/ H_2O , rt, 12 h/60 °C, 3 h; (viii) amine, PyAOP, DIPEA, DMF, rt, 12 h; (ix) amine, HATU, DIPEA, DMF, rt, 12 h.

The synthesis of hit 22 analogs 22–39 was achieved with a straightforward approach described in Scheme 2. Hydrazides (**e**) reacted with ethyl isothiocyanatoacetate in ACN to give thiosemihydrazides (**f**) that were converted to triazole acid derivatives (**g**) through in situ cyclization and hydrolysis when treated with aqueous NaOH. Amide coupling of these triazole acid derivatives (**g**) with various amines in the presence of HATU and DIPEA in DMF resulted in analogs 22–39.



Scheme 2. Synthetic Strategy for Analogs 22–39. Reagents and conditions: (i) ethyl isothiocyanatoacetate, ACN, 40 °C, 3 h; (ii) NaOH, H₂O, 100 °C, 3 h; (iii) Hydrazine, HATU, DIPEA, DMF, rt, 24 h.

2.1. Biology Cells

TZM-GFP cells are a modified version of TZM-bl cells and contain an integrated nlsGFP reporter gene under the transcriptional control of the HIV-1 long terminal repeat (LTR) [44,45]. TZM-GFP cells were kindly provided by Dr. Marc Johnson (University of Missouri-Columbia, Columbia, MO) and cultured in DMEM supplemented with 10% fetal bovine serum (FBS; Hyclone). HEK293-FT cells were also cultured in DMEM supplemented with 10% FBS. MT-2 cells were grown in RPMI supplemented with 10% heat-inactivated FBS. All cells were grown at 37 °C and maintained in humidified atmosphere containing 5% CO₂.

2.2. Method Details

2.2.1. Thermal Shift Assays (TSAs) to Screen Compounds for Effect on HIV-1 CA Hexamer Stability

Compounds were screened for their effect on CA hexamer stability using purified covalently-crosslinked hexameric CA^{A14C/E45C/W184A/M185A} (CA121). CA121 cloned in a pET11a expression plasmid was provided by Dr. Owen Pornillos (University of Virginia, Charlottesville, VA). Protein was expressed in *E. coli* BL21(DE3)RIL and purified as reported previously [26]. The TSA was conducted as previously described [46–48] using the PikoReal Real-Time PCR (Thermo Fisher Scientific, Waltham, MA, USA) or the QuantStudio 3 Real-Time PCR (Thermo Fisher Scientific) systems. Each reaction contained 10 µL of 15 µM CA121 (7.5 µM final concentration) in 50 mM sodium phosphate buffer (pH 8.0), 10 µL of 2× Sypro Orange Protein Gel Stain (Life Technologies, Carlsbad, CA, USA) in 50 mM sodium phosphate buffer (pH 8.0) and 0.2 µL of DMSO (control) or compound. Compounds were tested at a final concentration of 20 µM. The plate was heated from 25 to 95 °C with a heating rate of 0.2 °C/10 s. The fluorescence intensity was measured with an Ex range of 475–500 nm and Em range of 520–590 nm. The differences in the melting temperature (ΔT_m) of CA hexamer in DMSO (T_0) verses in the presence of compound (T_m) were calculated using the following formula: $\Delta T_m = T_m - T_0$.

2.2.2. Virus Production

The wild-type laboratory HIV-1 strain, HIV-1_{NL4-3} [49], was produced using a pNL4-3 vector that was obtained through the NIH AIDS Reagent Program. HIV-1_{NL4-3} was generated by transfecting HEK 293FT cells in a T75 flask with 10 µg of the pNL4-3 vector and FuGENE[®] HD Transfection Reagent (Promega, Madison, WI, USA). Supernatant was harvested 48–72 h post-transfection and transferred to MT2 cells for viral propagation. Virus was harvested when syncytia formation was observed, which took 3–5 days. The viral supernatant was then concentrated using 8% *w/v* PEG 8000 overnight at 4 °C, followed by centrifugation for 40 min at 3500 rpm. The resulting viral-containing pellet was concentrated 10-fold by resuspension in DMEM without FBS and stored at –80 °C.

2.2.3. Anti-HIV-1 and Cytotoxicity Assays

Anti-HIV-1 activity of PF74 and related analogs was examined in TZM-GFP cells. The potency of HIV-1 inhibition by a compound was based on its inhibitory effect on viral LTR-activated GFP expression compared with that of compound-free (DMSO) controls. Briefly, TZM-GFP cells were plated at density of 1×10^4 cells per well in a 96-well plate. 24 h later, media was replaced with increasing concentrations of compound. 24 h post treatment, cells were exposed to an HIV-1 strain (MOI = 1). After incubation for 48 h, anti-HIV-1 activity was assessed by counting the number of GFP positive

cells on a Cytation™ 5 Imaging Reader (BioTek, Winooski, VT, USA) and 50% effective concentration (EC₅₀) values were determined.

Cytotoxicity of each compound was also determined in TZM-GFP cells. Cells were plated at a density of 1×10^4 cells per well in a 96-well plate and were continuously exposed to increasing concentrations of a compound for 72 h. The number of viable cells in each well was determined using a Cell Proliferation Kit II (XTT), and 50% cytotoxicity concentration (CC₅₀) values were determined. All the cell-based assays were conducted in duplicate of at least two independent experiments and the average values were determined.

For calculation of EC₅₀ and CC₅₀ dose response curves, values were plotted in GraphPad Prism 5 and analyzed with the log (inhibitor) vs. normalized response—Variable slope equation. Final values were calculated in each independent assay and the average values were determined. Statistical analysis (calculation of standard deviation) was performed using Microsoft Excel.

2.3. Microsomal Stability Assay

The in vitro microsomal stability assay was conducted in duplicate in mouse and human liver microsomal systems, which were supplemented with nicotinamide adenine dinucleotide phosphate (NADPH) as a cofactor. Briefly, a compound (1 μ M final concentration) was pre-incubated, in the absence or presence of 0.5 μ M Cobicistat (CYP 3A inhibitor, purchased from medchemexpress.com and verified with LCMS), with the reaction mixture containing liver microsomal protein (0.5 mg/mL final concentration) and MgCl₂ (1 mM final concentration) in 0.1 M potassium phosphate buffer (pH 7.4) at 37 °C for 15 min. The reaction was initiated by addition of 1 mM NADPH, followed by incubation at 37 °C. A negative control was performed in parallel in the absence of NADPH to measure any chemical instability or non-NADPH dependent enzymatic degradation for each compound. At various time points (0, 5, 15, 30 and 60 min), 1 volume of reaction aliquot was taken and quenched with 3 volumes of acetonitrile containing an appropriate internal standard and 0.1% formic acid. The samples were then vortexed and centrifuged at 15,000 rpm for 5 min at 4 °C. The supernatants were collected and analyzed by LC-MS/MS to determine the in vitro metabolic half-life (t_{1/2}).

2.4. Molecular Modeling

Molecular modeling was performed using the Schrödinger small molecule drug discovery suite 2019-1 [50]. The crystal structure of native HIV-1 capsid protein in complex with PF74 [25] was retrieved from the protein data bank (PDB code: 4XFZ [25]). The above structure was analyzed using Maestro [51] (Schrödinger; LLC: New York, NY, USA) and subjected to a docking protocol that involves several steps including preparing protein of interest, grid generation, ligand preparation, and docking. The crystal structure was refined using the protein preparation wizard [52] (Schrödinger; LLC: New York, NY, USA.) wherein missing hydrogen atoms, side chains, and loops were added using Prime and minimized using the OPLS 3e force field [53] to optimize the hydrogen bonding network and converge the heavy atoms to an rmsd of 0.3 Å. The receptor grid generation tool in Maestro (Schrödinger; LLC: New York, NY, USA) was used to define an active site around the native ligand PF74 to cover all the residues within 12 Å. All the compounds were drawn using Maestro and subjected to Lig Prep to generate conformers, possible protonation at pH of 7 ± 2 that serves as an input for docking process. All the dockings were performed using Glide XP [54] (Glide: version 8.2) with the van der Waals radii of nonpolar atoms for each of the ligands were scaled by a factor of 0.8. The solutions were further refined by post docking and minimization under implicit solvent to account for protein flexibility. The residue numbers of HIV-1 capsid protein used in the discussion and the figures were based on the native HIV-1 capsid protein.

3. Results

All analogs synthesized for each hit were assessed first with a biophysical protein stability assay, or thermal shift assay, where the effect of the compound was measured by the change in protein melting point compared to the DMSO control (ΔT_m). A positive value in ΔT_m indicates a stabilizing

effect on the protein and a negative value indicates a destabilizing effect. Of note, the target CA protein is in a covalently crosslinked hexameric state. Thus, the ΔT_m values likely reflect local changes that may affect stabilization and exclude inter-hexamer effects, which are important correlates of overall capsid core stability. To simplify presentation of the data, we refer to the effects of these compounds as stabilization or destabilization of “CA hexamer.” All compounds were then screened at 20 μM against HIV-1 in a cell-based assay to determine antiviral activity. Compounds demonstrating significant inhibition were further tested in a dose-response fashion for antiviral EC_{50} values. All compounds were tested for cytotoxicity either by screening at 100 or 50 μM , or determination of CC_{50} values. The benchmark compound **PF74** was resynthesized and tested in these assays (1, $\Delta T_m = 7.4$ °C, $\text{EC}_{50} = 0.61$ μM , $\text{CC}_{50} = 76$ μM). The best compound (**10**) was also tested for liver microsomal stability. Molecular modeling was performed for a few selected compounds to help understand the SAR.

3.1. SAR of Hit 2 (R^1 and R^2)

Hit **2** showed only a weak CA hexamer stabilizing effect ($\Delta T_m = 0.5$ °C) with no significant antiviral activity at 20 μM and no cytotoxicity at 100 μM (Table 1). Removing the isopropyl group at R^1 (compound **3**) resulted in the complete loss of the CA hexamer stabilizing effect, whereas replacing it with an indole-7-methyl (compound **4**) did not yield significant differences in all three assays. When the ester was hydrolyzed to acid (compounds **5–7**), only the analog with an indole-7-methyl at R^1 (compound **5**) weakly stabilized CA hexamer ($\Delta T_m = 0.8$ °C); no such effect was observed when R^1 was a benzyl methyl thioether (compound **6**) or a bulky alkyl (compound **7**). Amidation of the acid with an aniline yielded more structurally elaborate analogs **8–10**. Of these, the analogs with a benzyl methyl thioether (compound **8**) or an indole-7-methyl (compound **9**) at R^1 showed only weak CA hexamer stabilization ($\Delta T_m = 0.5$ °C for both), whereas a much stronger CA hexamer stabilizing effect was observed with compound **10** which bears a benzyl moiety at R^1 ($\Delta T_m = 2.5$ °C). More importantly, compound **10** inhibited HIV-1 with a potency ($\text{EC}_{50} = 1.6$ μM) only 2.5-fold less than **PF74** ($\text{EC}_{50} = 0.61$ μM). In addition, compound **10** ($\text{CC}_{50} > 100$ μM) was less cytotoxic than **PF74** ($\text{CC}_{50} = 76$ μM).

Table 1. Anti-HIV-1 activity, cytotoxicity, and CA hexamer stability profiles of **2–10** (R^1 , R^2).

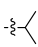
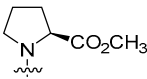
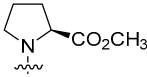
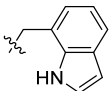
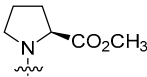
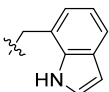
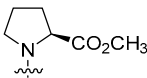
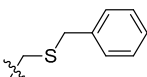
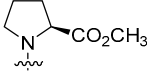
Compd	R^1	R^2	EC_{50} (μM) ^[a]	CC_{50} (μM) ^[b]	TSA ΔT_m (°C) ^[c]
1 (PF74)	–	–	0.61 ± 0.2	76 ± 9	7.4
2			>20	>100	0.5
3	H		>20	>100	0
4			>20	<100	0.5
5			>20	>100	0.8
6			>20	>100	0

Table 1. Cont.

Compd	R ¹	R ²	EC ₅₀ (μM) ^[a]	CC ₅₀ (μM) ^[b]	TSA ΔTm (°C) ^[c]
7			>20	>100	0
8			>20	44 ± 5	0.5
9			>20	>100	0.5
10			1.6 ± 0.1	>100	2.5

^a Concentration of compound inhibiting HIV-1 replication by 50%, expressed as the mean ± standard deviation from at least two independent experiments. ^b Concentration of compound causing 50% cell death, expressed as the mean ± standard deviation from at least two independent experiments. ^c TSA: thermal shift assay. ΔTm: change of CA crosslinked hexamer melting point in the presence of compound minus DMSO control.

3.2. SAR of Hit 11 (R¹, R³, and R⁴)

Hit **11** was designed from hit **2** and **PF74** via molecular hybridization. As a result, the skeleton of **11** is very similar to that of **PF74**, except that the indole moiety was replaced with a bioisosteric quinazoline-2,4-dione moiety. A general SAR observation was that when R¹ was a bulky alkyl group, compounds (**14–21**) did not show significant antiviral activity at 20 μM or cytotoxicity at 100 μM (Table 2), though most analogs weakly stabilized CA hexamer (ΔTm = 0.5–0.7 °C). However, when R¹ was a benzyl group to mimic **PF74**, the activity profiles changed substantially (analog **11–13**) and demonstrated a strong dependence on R³. When R³ was a methyl group, analog **11** (ΔTm = 2.7 °C, EC₅₀ = 6.9 μM) and analog **13** (ΔTm = 2.4 °C, EC₅₀ = 8.0 μM) both moderately stabilized CA hexamer and inhibited HIV-1, without observed cytotoxicity (CC₅₀ >100 μM). By contrast, when R³ was a hydrogen, the resulting analog (**12**) did not show activity in either assay. Overall, SARs around R¹ and R³ within this series strongly indicate that both the benzyl group at R¹ and the methyl group at R³ are important for potency.

Table 2. Anti-HIV-1 activity, cytotoxicity, and CA hexamer stability profiles of **11–21** (R¹, R³, and R⁴).

Compd	R ¹	R ³	R ⁴	EC ₅₀ (μM) ^[a]	CC ₅₀ (μM) ^[b]	TSA ΔTm (°C) ^[c]
1 (PF74)	–	–	–	0.61 ± 0.2	76 ± 9	7.4
11		Me	H	6.9 ± 0.8	>100	2.7
12		H	H	>20	<100	0
13		Me	F	8.0 ± 1.3	>100	2.4
14		Me	H	>20	>100	0
15		H	H	>20	>100	0.7
16		Me	Me	>20	>100	0
17		H	H	>20	>100	0
18		Me	H	>20	>100	0.5

Table 2. Cont.

Compd	R ¹	R ³	R ⁴	EC ₅₀ (μM) [a]	CC ₅₀ (μM) [b]	TSA ΔTm (°C) [c]
19		H	H	>20	>100	0.6
20		Me	Cl	>20	>100	0.5
21		H		>20	>100	0.6

^a Concentration of compound inhibiting HIV-1 replication by 50%, expressed as the mean ± standard deviation from at least two independent experiments. ^b Concentration of compound causing 50% cell death, expressed as the mean ± standard deviation from at least two independent experiments. ^c TSA: thermal shift assay. ΔTm: change of CA crosslinked hexamer melting point in the presence of compound minus DMSO control.

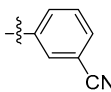
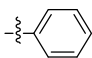
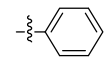
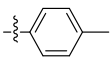
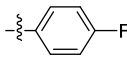
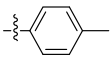
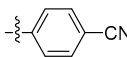
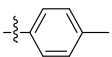
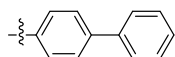
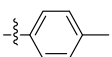
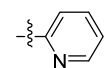
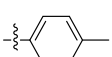
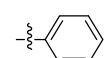
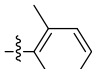
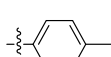
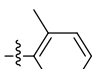
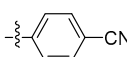
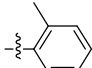
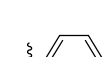
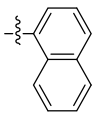
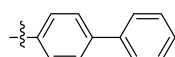
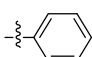
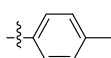
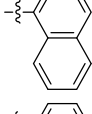
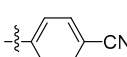
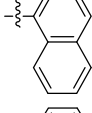
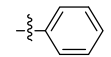
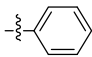
3.3. SAR of Hit 22 (R⁵, R⁶, and R⁷)

Compound **22** is structurally quite different from **PF74** and the other two hits (**2** and **11**), though it satisfied multiple pharmacophore points (Figure 2A), and hence, could be similar to **PF74** in 3D shape. In addition, the 1,2,4-triazole is a well-known bioisostere [55] of carboxamide, which renders **22** functionally similar to **PF74**. The SARs of this series were centered around the two aromatic rings (R⁵ and R⁷). The most prominent observation was that analogs within this series did not significantly inhibit HIV-1 at 20 μM, and did not show cytotoxicity at 100 μM (Table 3). However, with the exception of **23**, **32**, and **33**, all analogs demonstrated an impact on CA hexamer stability, which essentially validates our hit generation approach as the shape similarity search is target-based. Very interestingly, a weak CA hexamer destabilizing effect, rather than stabilizing effect, was observed with hit **22** (ΔTm = −0.5 °C). A similar destabilizing effect was also observed with the only other analog featuring a pyridine ring at R⁵ (compound **31**), though the effect was significantly more prominent (ΔTm = −1.2 °C). All other analogs feature either a phenyl or a biphenyl ring at R⁵, and in stark contrast, produced CA hexamer stabilizing effect (ΔTm = 0.5–0.9 °C). This weak stabilizing effect was not impacted by functional group substitution at either R⁵ or R⁷. Finally, N-methyl substitution of analog **23** (ΔTm = 0 °C) yielded a compound **39** stabilizing CA hexamer (ΔTm = 1.2 °C). These observations strongly indicate that (1) pyridine at R⁵ destabilizes the CA hexamer whereas a phenyl or biphenyl moiety at R⁵ stabilizes the CA hexamer; (2) a methyl group at the para position of the phenyl ring at R⁷ reinforces the destabilizing effect (**31** vs. **22**) but does not impact the stabilizing effect (**28** vs. **24**, **30** vs. **36**); and (3) a methyl group at R⁶ confers a CA hexamer stabilizing effect (**39** vs. **23**).

Table 3. Anti-HIV-1 activity, cytotoxicity, and CA hexamer stability profiles of **22–39** (R⁵, R⁶, and R⁷).

Compd	R ⁵	R ⁶	R ⁷	EC ₅₀ (μM) [a]	CC ₅₀ (μM) [b]	TSA ΔTm (°C) [c]
22		H		>20	>100	−0.5
23		H		>20	>100	0
24		H		>20	>100	0.7
25		H		>20	>100	0.6

Table 3. Cont.

Compd	R ⁵	R ⁶	R ⁷	EC ₅₀ (μM) ^[a]	CC ₅₀ (μM) ^[b]	TSA ΔTm (°C) ^[c]
26		H		>20	>100	0.7
27		H		>20	~100	0.7
28		H		>20	>100	0.7
29		H		>20	>100	0
30		H		>20	>100	0.8
31		H		>20	>100	-1.2
32		H		>20	>100	0
33		H		>20	>100	0
34		H		>20	>100	0.6
35		H		>20	>100	0.5
36		H		>20	>100	0.8
37		H		>20	>100	1.0
38		H		>20	>100	0.9
39		Me		>20	>50	1.2

^a Concentration of compound inhibiting HIV-1 replication by 50%, expressed as the mean ± standard deviation from at least two independent experiments. ^b Concentration of compound causing 50% cell death, expressed as the mean ± standard deviation from at least two independent experiments. ^c TSA: thermal shift assay. ΔTm: change of CA crosslinked hexamer melting point in the presence of compound minus DMSO control.

3.4. Metabolic Stability

To characterize the drug-like property of **10**, our most potent antiviral compound from the current work, we conducted metabolic stability assays in both HLMs and mouse liver microsomes (MLMs). Metabolic stability is a major absorption, distribution, metabolism and excretion (ADME) property that profoundly impacts drug bioavailability [56]. Peptidomimetics are particularly susceptible to phase I metabolism, presumably because they are good substrates [57] for liver metabolizing enzyme subfamily cytochrome P450 3A (CYP3A), which is responsible for the metabolism of at least 50% of all current drugs [58]. It is known that **PF74** is a severely flawed antiviral lead due to its prohibitively low metabolic stability [34]. This was confirmed in our metabolic stability assays, where the half-life ($t_{1/2}$) of **PF74** is less than 1 min in both HLMs and MLMs (Table 4). By contrast, our compound **10** was decisively more stable, particularly in HLMs where its half-life ($t_{1/2} = 31$ min) was 44-fold longer than

that of **PF74** ($t_{1/2} = 0.7$ min). When tested in combination with a CYP3A inhibitor Cobicistat (Cobi) [59], **10** still exhibited significantly longer half-life than that of **PF74**. A $t_{1/2} > 30$ min in HLM generally indicates good in vivo metabolic stability and oral bioavailability. Collectively, these observations support our compound **10** as a viable antiviral hit, and corroborate the hypothesis that the poor metabolic stability of **PF74** is due to CYP3A-mediated phase I metabolism.

Table 4. Phase I metabolic stability in liver microsomes $t_{1/2}$ (min).

Compound	HLM ^a	HLM ^a (+Cobi ^c)	MLM ^b	MLM ^b (+Cobi ^c)
PF74	0.7	91	0.6	34
10	31	>120	2.9	85
Verapamil	15	–	4.2	–

^a HLM: human liver microsome; ^b MLM: mouse liver microsome; ^c Microsomal stability measured in the presence of CYP3A inhibitor Cobi.

3.5. Molecular Modeling

To understand some of the aforementioned SAR, we performed molecular modeling with selected compounds based on the co-crystal structure of native HIV-1 capsid protein bound to **PF74** (PDB code: 4XFZ [25]). Compound **11** (Figure 3A) bearing a quinazoline-2,4(1*H*,3*H*)-dione core in place of the indole ring of **PF74** interacted with the same key residues in the CA hexamer as **PF74**. Observed key interactions included (i) hydrogen-bonding between N57 and the NH and carbonyl groups of the phenylalanine fragment on compound **11**, between K70 and the carbonyl next to the phenylalanine fragment of **11**, and between Q63 and the free NH of the quinazoline-2,4(1*H*,3*H*)-dione core of **11**; (ii) cation- π interactions between protonated K70 and quinazoline-2,4(1*H*,3*H*)-dione aromatic ring. However, despite sharing the same binding site and similar key interactions, compound **11** was significantly less potent than **PF74**. In the meantime, a complete loss in potency was observed for leucine derived analog **14**, which could be attributed to its shifting away from the binding site (circled), possibly in a binding mode shown in Figure 3B, and hence the loss of key interactions. This observation signified the importance of the phenylalanine core of these compounds for potency. In particular, the benzyl group of the phenylalanine core could play an important role in keeping a molecule inside the **PF74**-bound cavity through hydrophobic interactions [25] with surrounding residues L56, M66, and L69, as evident from the observed binding mode for compound **11** (Figure 3A). This was consistent with the significant increase in the potency of compound **10** as well, which bears a benzyl group and an additional *L*-proline core. Like the **PF74** backbone, the benzyl group of the phenylalanine fragment forces compound **10** to nestle in the cavity in such a way that the aniline ring of the *L*-proline core is extended to the adjacent CA_{NTD} domain, resulting in an additional hydrogen-bonding between the carbonyl of the *L*-proline and NH₂ of N53, along with the typical H-bonding with N57, Q63, and K70 (Figure 3C). Additionally, pyrrolidine core of *L*-proline is oriented in such a way that it has maximum interaction with A105, T107, and Y130. Expectedly, introduction of an *L*-cysteine derived core having an elongated backbone in place of phenylalanine in compound **8** forces the entire molecule out of the cavity, diminishing its potency (Figure 3D). Compound **8** was found to be closer to the adjacent CA_{CTD} and CA_{NTD} domains, interacting with P34, R173, Q179, and K182 through H-bonding.

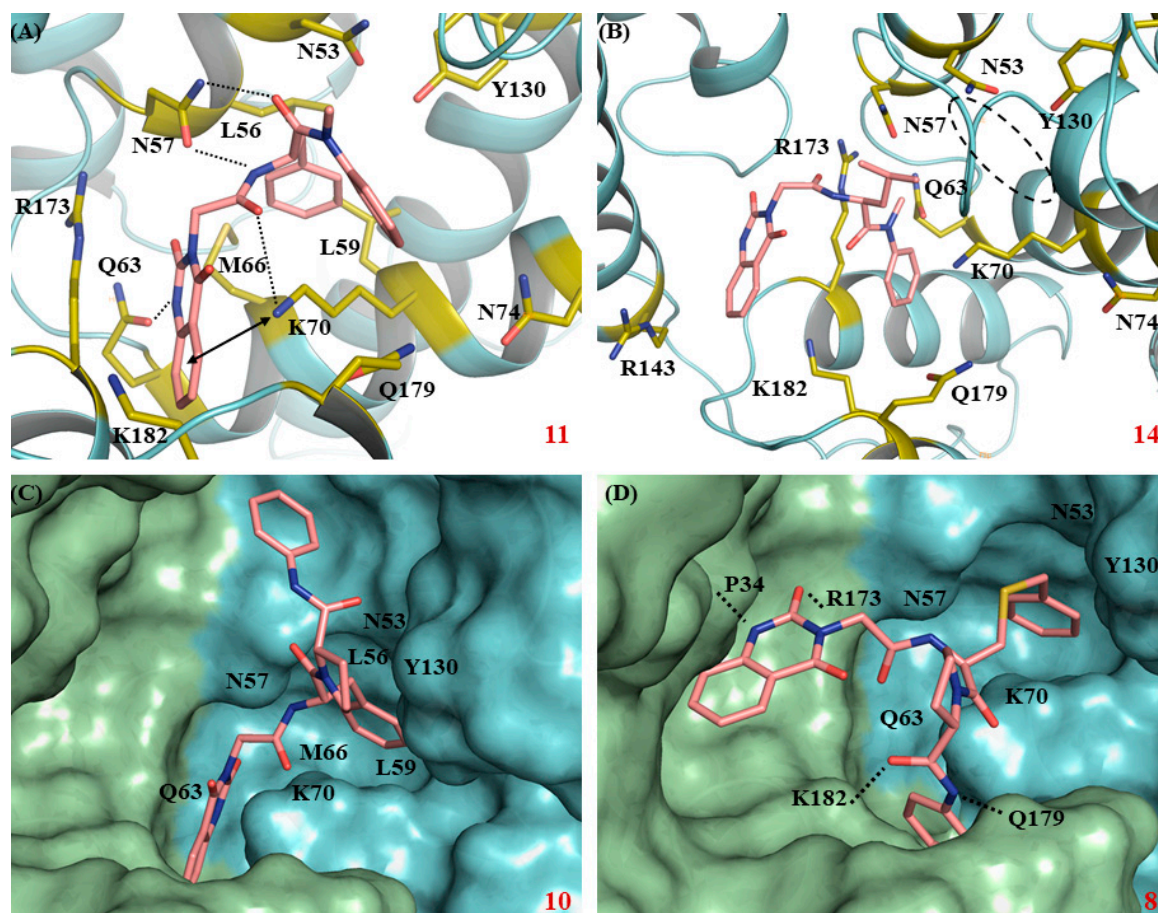


Figure 3. Docking poses of key ligands based on native HIV-1 capsid protein bound to PF74 (PDB code: 4XFZ [25]). (A) Predicted binding mode of **11**. Glide score (kcal/mol): -6.3 . (B) Predicted binding mode of **14** away from the preferred binding site (circled). Glide scores (kcal/mol): -4.2 . (C) Predicted binding and fitting of *L*-proline analog **10** within the preferred PF74 binding cavity. Glide score (kcal/mol): -6.3 . (D) Predicted binding and fitting of *L*-cysteine derivative analog **8** away from the preferred PF74 binding site. Glide score (kcal/mol): -5.2 . Ligands numbers **8**, **10**, **11**, and **14** are in pink. In Figure A and D, H-bond and cation- π interactions are depicted as black dotted lines and double headed arrow, respectively. In (A) and (B), the capsid protein chain is colored cyan and key residues around binding site are colored olive. In (C) and (D), CA_{NTD} around helices H3 and H4 in chain A are colored cyan, and CA_{CTD} around helices H8 and H9 in the adjacent chain B are colored green. The nitrogen, oxygen, and sulfur atoms are colored blue, red, and yellow, respectively.

4. Discussion

Despite the approval of many HIV-1 antiviral regimens [60], a curative therapy remains elusive and HIV-1 continues to pose a global healthcare challenge. There is a need to develop new classes of HIV-1 drugs with distinct mechanisms of action to manage HIV-1 strains resistant to current drugs. The multifunctional HIV-1 CA represents an attractive target for novel antiviral discovery. PF74 is a CA-targeting small molecule which binds to a unique pocket between a viral CA_{NTD} and the adjacent CA_{CTD}, and competes against a few host factors important for viral replication. The antiviral profile of PF74 and its mode of CA binding are well characterized. However, PF74 is not a viable antiviral lead as it suffers from extremely low metabolic stability. Aiming to identify mechanistically similar yet structurally distinct small molecules with improved metabolic stability, we performed a pharmacophore-based shape similarity search based on PF74. Subsequently, we conducted analog synthesis and SAR for two hits (**2** and **22**) generated from the shape similarity search, as well as a third hit (**11**) designed via molecular hybridization. Overall, most of analogs exhibited weak yet discernible

impacts on the stability of CA hexamer, which largely validates our hit generation approach. Three of the analogs (**10**, **11**, and **13**) showed moderate CA hexamer stabilizing effects and significant anti-HIV-1 activities. Particularly, compound **10** inhibited HIV-1 with an EC₅₀ of 1.6 μM, which is only 2.5-fold less potent than **PF74**. More importantly, compound **10** demonstrated drastically improved metabolic stability over **PF74** in HLMs (t_{1/2} = 31 min for **10** vs. 0.7 min for **PF74**). Molecular modeling indicates that our compound **10** binds comfortably in the **PF74** binding pocket. Collectively, our data support **10** as a potent and metabolically stable HIV-1 CA-targeting antiviral lead.

Supplementary Materials: The following are available online at <http://www.mdpi.com/1999-4915/12/4/452/s1>, Scheme S1: Synthesis of intermediates **b–d**, and compounds **2–21**, Scheme S2: Synthesis of intermediates **f–g** and compounds **22–39**.

Author Contributions: S.G.S. and Z.W. conceptualized the research. S.K.V.V., R.L.S., and L.W. designed, synthesized and characterized all compounds. J.K. performed the shape similarity search. R.L.S. conducted molecular docking. J.X. performed the metabolic stability assays. M.C.C., K.A.K., H.D., H.Z., and P.R.T. performed T.S.A., antiviral and cytotoxicity assays. R.L.S. and Z.W. wrote the manuscript. All authors have read and agreed to the published version of the manuscript.

Funding: This research was funded by the National Institute of Allergy and Infectious Diseases, the National Institute of Health, grant number R01AI120860 (to SGS and ZW).

Acknowledgments: We thank the Minnesota Supercomputing Institute (MSI) at the University of Minnesota for providing molecular modeling resources.

Conflicts of Interest: The authors declare no conflict of interest.

References

1. Freed, E.O. HIV-1 assembly, release and maturation. *Nat. Rev. Microbiol.* **2015**, *13*, 484–496. [[CrossRef](#)]
2. Ganser, B.K.; Li, S.; Klishko, V.Y.; Finch, J.T.; Sundquist, W.I. Assembly and analysis of conical models for the HIV-1 core. *Science* **1999**, *283*, 80–83. [[CrossRef](#)] [[PubMed](#)]
3. Li, S.; Hill, C.P.; Sundquist, W.I.; Finch, J.T. Image reconstructions of helical assemblies of the HIV-1 CA protein. *Nature* **2000**, *407*, 409–413. [[CrossRef](#)] [[PubMed](#)]
4. Campbell, E.M.; Hope, T.J. HIV-1 capsid: The multifaceted key player in HIV-1 infection. *Nat. Rev. Microbiol.* **2015**, *13*, 471–483. [[CrossRef](#)] [[PubMed](#)]
5. Sundquist, W.I.; Krausslich, H.G. HIV-1 assembly, budding, and maturation. *Cold Spring Harb. Perspect. Med.* **2012**, *2*, a006924. [[CrossRef](#)]
6. Le Sage, V.; Moulard, A.J.; Valiente-Echeverria, F. Roles of HIV-1 capsid in viral replication and immune evasion. *Virus Res.* **2014**, *193*, 116–129. [[CrossRef](#)] [[PubMed](#)]
7. Hilditch, L.; Towers, G.J. A model for cofactor use during HIV-1 reverse transcription and nuclear entry. *Curr. Opin. Virol.* **2014**, *4*, 32–36. [[CrossRef](#)]
8. Ambrose, Z.; Aiken, C. HIV-1 uncoating: Connection to nuclear entry and regulation by host proteins. *Virology* **2014**, *454–455*, 371–379. [[CrossRef](#)]
9. Stremlau, M.; Owens, C.M.; Perron, M.J.; Kiessling, M.; Autissier, P.; Sodroski, J. The cytoplasmic body component TRIM5α restricts HIV-1 infection in Old World monkeys. *Nature* **2004**, *427*, 848–853. [[CrossRef](#)]
10. Sayah, D.M.; Sokolskaja, E.; Berthou, L.; Luban, J. Cyclophilin A retrotransposition into TRIM5 explains owl monkey resistance to HIV-1. *Nature* **2004**, *430*, 569–573. [[CrossRef](#)]
11. Achuthan, V.; Perreira, J.M.; Sowd, G.A.; Puray-Chavez, M.; McDougall, W.M.; Paulucci-Holthausen, A.; Wu, X.; Fadel, H.J.; Poeschla, E.M.; Multani, A.S.; et al. Capsid-CPSF6 Interaction Licenses Nuclear HIV-1 Trafficking to Sites of Viral DNA Integration. *Cell Host Microbe* **2018**, *24*, 392–404.e8. [[CrossRef](#)] [[PubMed](#)]
12. Bejarano, D.A.; Peng, K.; Laketa, V.; Borner, K.; Jost, K.L.; Lucic, B.; Glass, B.; Lucic, M.; Mueller, B.; Krausslich, H.G. HIV-1 nuclear import in macrophages is regulated by CPSF6-capsid interactions at the nuclear pore complex. *Elife* **2019**, *8*, e41800. [[CrossRef](#)] [[PubMed](#)]
13. Woodward, C.L.; Prakobwanakit, S.; Mosessian, S.; Chow, S.A. Integrase interacts with nucleoporin NUP153 to mediate the nuclear import of human immunodeficiency virus type 1. *J. Virol.* **2009**, *83*, 6522–6533. [[CrossRef](#)] [[PubMed](#)]

14. Matreyek, K.A.; Yucel, S.S.; Li, X.; Engelman, A. Nucleoporin NUP153 phenylalanine-glycine motifs engage a common binding pocket within the HIV-1 capsid protein to mediate lentiviral infectivity. *PLoS Pathog.* **2013**, *9*, e1003693. [[CrossRef](#)]
15. Buffone, C.; Martinez-Lopez, A.; Fricke, T.; Opp, S.; Severgnini, M.; Cifola, I.; Petiti, L.; Frabetti, S.; Skorupka, K.; Zadrozny, K.K.; et al. Nup153 Unlocks the Nuclear Pore Complex for HIV-1 Nuclear Translocation in Nondividing Cells. *J. Virol.* **2018**, *92*, e00648-18. [[CrossRef](#)]
16. Meehan, A.M.; Saenz, D.T.; Guevera, R.; Morrison, J.H.; Peretz, M.; Fadel, H.J.; Hamada, M.; van Deursen, J.; Poeschla, E.M. A cyclophilin homology domain-independent role for Nup358 in HIV-1 infection. *PLoS Pathog.* **2014**, *10*, e1003969. [[CrossRef](#)]
17. Dharan, A.; Talley, S.; Tripathi, A.; Mamede, J.I.; Majetschak, M.; Hope, T.J.; Campbell, E.M. KIF5B and Nup358 Cooperatively Mediate the Nuclear Import of HIV-1 during Infection. *PLoS Pathog.* **2016**, *12*, e1005700. [[CrossRef](#)]
18. Mamede, J.I.; Damond, F.; Bernardo, A.; Matheron, S.; Descamps, D.; Battini, J.L.; Sitbon, M.; Courgnaud, V. Cyclophilins and nucleoporins are required for infection mediated by capsids from circulating HIV-2 primary isolates. *Sci. Rep.* **2017**, *7*, 45214. [[CrossRef](#)]
19. Fricke, T.; White, T.E.; Schulte, B.; de Souza Aranha Vieira, D.A.; Dharan, A.; Campbell, E.M.; Brandariz-Nunez, A.; Diaz-Griffero, F. MxB binds to the HIV-1 core and prevents the uncoating process of HIV-1. *Retrovirology* **2014**, *11*, 68. [[CrossRef](#)]
20. Xu, B.; Pan, Q.; Liang, C. Role of MxB in Alpha Interferon-Mediated Inhibition of HIV-1 Infection. *J. Virol.* **2018**, *92*, e00422-18. [[CrossRef](#)]
21. Kim, K.; Dauphin, A.; Komurlu, S.; McCauley, S.M.; Yurkovetskiy, L.; Carbone, C.; Diehl, W.E.; Strambio-De-Castillia, C.; Campbell, E.M.; Luban, J. Cyclophilin A protects HIV-1 from restriction by human TRIM5alpha. *Nat. Microbiol.* **2019**, *4*, 2044–2051. [[CrossRef](#)]
22. Franke, E.K.; Yuan, H.E.; Luban, J. Specific incorporation of cyclophilin A into HIV-1 virions. *Nature* **1994**, *372*, 359–362. [[CrossRef](#)] [[PubMed](#)]
23. Thali, M.; Bukovsky, A.; Kondo, E.; Rosenwirth, B.; Walsh, C.T.; Sodroski, J.; Gottlinger, H.G. Functional association of cyclophilin A with HIV-1 virions. *Nature* **1994**, *372*, 363–365. [[CrossRef](#)] [[PubMed](#)]
24. Novikova, M.; Zhang, Y.; Freed, E.O.; Peng, K. Multiple Roles of HIV-1 Capsid during the Virus Replication Cycle. *Virol. Sin.* **2019**, *34*, 119–134. [[CrossRef](#)]
25. Gres, A.T.; Kirby, K.A.; KewalRamani, V.N.; Tanner, J.J.; Pornillos, O.; Sarafianos, S.G. STRUCTURAL VIROLOGY. X-ray crystal structures of native HIV-1 capsid protein reveal conformational variability. *Science* **2015**, *349*, 99–103. [[CrossRef](#)] [[PubMed](#)]
26. Pornillos, O.; Ganser-Pornillos, B.K.; Kelly, B.N.; Hua, Y.; Whitby, F.G.; Stout, C.D.; Sundquist, W.I.; Hill, C.P.; Yeager, M. X-ray structures of the hexameric building block of the HIV capsid. *Cell* **2009**, *137*, 1282–1292. [[CrossRef](#)] [[PubMed](#)]
27. Zhao, G.; Perilla, J.R.; Yufenyuy, E.L.; Meng, X.; Chen, B.; Ning, J.; Ahn, J.; Gronenborn, A.M.; Schulten, K.; Aiken, C.; et al. Mature HIV-1 capsid structure by cryo-electron microscopy and all-atom molecular dynamics. *Nature* **2013**, *497*, 643–646. [[CrossRef](#)]
28. Goudreau, N.; Lemke, C.T.; Faucher, A.M.; Grand-Maitre, C.; Goulet, S.; Lacoste, J.E.; Rancourt, J.; Malenfant, E.; Mercier, J.F.; Titolo, S.; et al. Novel inhibitor binding site discovery on HIV-1 capsid N-terminal domain by NMR and X-ray crystallography. *ACS Chem. Biol.* **2013**, *8*, 1074–1082. [[CrossRef](#)]
29. Price, A.J.; Jacques, D.A.; McEwan, W.A.; Fletcher, A.J.; Essig, S.; Chin, J.W.; Halambage, U.D.; Aiken, C.; James, L.C. Host cofactors and pharmacologic ligands share an essential interface in HIV-1 capsid that is lost upon disassembly. *PLoS Pathog.* **2014**, *10*, e1004459. [[CrossRef](#)]
30. Bhattacharya, A.; Alam, S.L.; Fricke, T.; Zadrozny, K.; Sedzicki, J.; Taylor, A.B.; Demeler, B.; Pornillos, O.; Ganser-Pornillos, B.K.; Diaz-Griffero, F.; et al. Structural basis of HIV-1 capsid recognition by PF74 and CPSF6. *Proc. Natl. Acad. Sci. USA* **2014**, *111*, 18625–18630. [[CrossRef](#)]
31. Sowd, G.A.; Serrao, E.; Wang, H.; Wang, W.; Fadel, H.J.; Poeschla, E.M.; Engelman, A.N. A critical role for alternative polyadenylation factor CPSF6 in targeting HIV-1 integration to transcriptionally active chromatin. *Proc. Natl. Acad. Sci. USA* **2016**, *113*, E1054–E1063. [[CrossRef](#)] [[PubMed](#)]
32. Shi, J.; Zhou, J.; Shah, V.B.; Aiken, C.; Whitby, K. Small-molecule inhibition of human immunodeficiency virus type 1 infection by virus capsid destabilization. *J. Virol.* **2011**, *85*, 542–549. [[CrossRef](#)] [[PubMed](#)]

33. Saito, A.; Ferhadian, D.; Sowd, G.A.; Serrao, E.; Shi, J.; Halambage, U.D.; Teng, S.; Soto, J.; Siddiqui, M.A.; Engelman, A.N.; et al. Roles of Capsid-Interacting Host Factors in Multimodal Inhibition of HIV-1 by PF74. *J. Virol.* **2016**, *90*, 5808–5823. [[CrossRef](#)] [[PubMed](#)]
34. Xu, J.P.; Francis, A.C.; Meuser, M.E.; Mankowski, M.; Ptak, R.G.; Rashad, A.A.; Melikyan, G.B.; Cocklin, S. Exploring Modifications of an HIV-1 Capsid Inhibitor: Design, Synthesis, and Mechanism of Action. *J. Drug Des. Res.* **2018**, *5*, 1070. [[PubMed](#)]
35. Sun, L.; Huang, T.; Dick, A.; Meuser, M.E.; Zalloum, W.A.; Chen, C.H.; Ding, X.; Gao, P.; Cocklin, S.; Lee, K.H.; et al. Design, synthesis and structure-activity relationships of 4-phenyl-1H-1,2,3-triazole phenylalanine derivatives as novel HIV-1 capsid inhibitors with promising antiviral activities. *Eur. J. Med. Chem.* **2020**, *190*, 112085. [[CrossRef](#)] [[PubMed](#)]
36. Wu, G.; Zalloum, W.A.; Meuser, M.E.; Jing, L.; Kang, D.; Chen, C.H.; Tian, Y.; Zhang, F.; Cocklin, S.; Lee, K.H.; et al. Discovery of phenylalanine derivatives as potent HIV-1 capsid inhibitors from click chemistry-based compound library. *Eur. J. Med. Chem.* **2018**, *158*, 478–492. [[CrossRef](#)]
37. Kubinyi, H. Similarity and dissimilarity: A medicinal chemist's view. *Perspect. Drug Discov.* **1998**, *9–11*, 225–252. [[CrossRef](#)]
38. Maggiora, G.; Vogt, M.; Stumpfe, D.; Bajorath, J. Molecular similarity in medicinal chemistry. *J. Med. Chem.* **2014**, *57*, 3186–3204. [[CrossRef](#)]
39. Sterling, T.; Irwin, J.J. ZINC 15—Ligand Discovery for Everyone. *J. Chem. Inf. Model.* **2015**, *55*, 2324–2337. [[CrossRef](#)]
40. Dixon, S.L.; Smondryev, A.M.; Rao, S.N. PHASE: A novel approach to pharmacophore modeling and 3D database searching. *Chem. Biol. Drug Des.* **2006**, *67*, 370–372. [[CrossRef](#)]
41. Dixon, S.L.; Smondryev, A.M.; Knoll, E.H.; Rao, S.N.; Shaw, D.E.; Friesner, R.A. PHASE: A new engine for pharmacophore perception, 3D QSAR model development, and 3D database screening: 1. Methodology and preliminary results. *J. Comput. Aided Mol. Des.* **2006**, *20*, 647–671. [[CrossRef](#)] [[PubMed](#)]
42. Lipinski, C.A. Lead- and drug-like compounds: The rule-of-five revolution. *Drug Discov. Today Technol.* **2004**, *1*, 337–341. [[CrossRef](#)] [[PubMed](#)]
43. Harrison, J.R.; Brand, S.; Smith, V.; Robinson, D.A.; Thompson, S.; Smith, A.; Davies, K.; Mok, N.; Torrie, L.S.; Collie, I.; et al. A Molecular Hybridization Approach for the Design of Potent, Highly Selective, and Brain-Penetrant N-Myristoyltransferase Inhibitors. *J. Med. Chem.* **2018**, *61*, 8374–8389. [[CrossRef](#)] [[PubMed](#)]
44. Lange, M.J.; Lyddon, T.D.; Johnson, M.C. Diphtheria Toxin A-Resistant Cell Lines Enable Robust Production and Evaluation of DTA-Encoding Lentiviruses. *Sci. Rep.* **2019**, *9*, 8985. [[CrossRef](#)]
45. Rosa, A.; Chande, A.; Ziglio, S.; De Sanctis, V.; Bertorelli, R.; Goh, S.L.; McCauley, S.M.; Nowosielska, A.; Antonarakis, S.E.; Luban, J.; et al. HIV-1 Nef promotes infection by excluding SERINC5 from virion incorporation. *Nature* **2015**, *526*, 212–217. [[CrossRef](#)]
46. Lo, M.C.; Aulabaugh, A.; Jin, G.; Cowling, R.; Bard, J.; Malamas, M.; Ellestad, G. Evaluation of fluorescence-based thermal shift assays for hit identification in drug discovery. *Anal. Biochem.* **2004**, *332*, 153–159. [[CrossRef](#)]
47. Miyazaki, Y.; Doi, N.; Koma, T.; Adachi, A.; Nomaguchi, M. Novel In Vitro Screening System Based on Differential Scanning Fluorimetry to Search for Small Molecules against the Disassembly or Assembly of HIV-1 Capsid Protein. *Front. Microbiol.* **2017**, *8*, 1413. [[CrossRef](#)]
48. Pantoliano, M.W.; Petrella, E.C.; Kwasnoski, J.D.; Lobanov, V.S.; Myslik, J.; Graf, E.; Carver, T.; Asel, E.; Springer, B.A.; Lane, P.; et al. High-density miniaturized thermal shift assays as a general strategy for drug discovery. *J. Biomol. Screen.* **2001**, *6*, 429–440. [[CrossRef](#)]
49. Adachi, A.; Gendelman, H.E.; Koenig, S.; Folks, T.; Willey, R.; Rabson, A.; Martin, M.A. Production of acquired immunodeficiency syndrome-associated retrovirus in human and nonhuman cells transfected with an infectious molecular clone. *J. Virol.* **1986**, *59*, 284–291. [[CrossRef](#)]
50. Schrodinger. *Schrödinger Small-Molecule Drug Discovery Suite 2015-4*, Schrödinger; LLC: New York, NY, USA, 2015.
51. Schrodinger. *Schrödinger Release 2020-1: Maestro*, Schrödinger; LLC: New York, NY, USA, 2020.
52. Sastry, G.M.; Adzhigirey, M.; Day, T.; Annabhimoju, R.; Sherman, W. Protein and ligand preparation: Parameters, protocols, and influence on virtual screening enrichments. *J. Comput. Aid Mol. Des.* **2013**, *27*, 221–234. [[CrossRef](#)]

53. Jorgensen, W.L.; Maxwell, D.S.; TiradoRives, J. Development and testing of the OPLS all-atom force field on conformational energetics and properties of organic liquids. *J. Am. Chem. Soc.* **1996**, *118*, 11225–11236. [[CrossRef](#)]
54. Friesner, R.A.; Murphy, R.B.; Repasky, M.P.; Frye, L.L.; Greenwood, J.R.; Halgren, T.A.; Sanschagrin, P.C.; Mainz, D.T. Extra precision glide: Docking and scoring incorporating a model of hydrophobic enclosure for protein-ligand complexes. *J. Med. Chem.* **2006**, *49*, 6177–6196. [[CrossRef](#)] [[PubMed](#)]
55. Meanwell, N.A. Synopsis of some recent tactical application of bioisosteres in drug design. *J. Med. Chem.* **2011**, *54*, 2529–2591. [[CrossRef](#)] [[PubMed](#)]
56. Masimirembwa, C.M.; Bredberg, U.; Andersson, T.B. Metabolic stability for drug discovery and development: Pharmacokinetic and biochemical challenges. *Clin. Pharmacokinet.* **2003**, *42*, 515–528. [[CrossRef](#)] [[PubMed](#)]
57. Wachter, V.J.; Silverman, J.A.; Zhang, Y.; Benet, L.Z. Role of P-glycoprotein and cytochrome P450 3A in limiting oral absorption of peptides and peptidomimetics. *J. Pharm. Sci.* **1998**, *87*, 1322–1330. [[CrossRef](#)] [[PubMed](#)]
58. Eichelbaum, M.; Burk, O. CYP3A genetics in drug metabolism. *Nat. Med.* **2001**, *7*, 285–287. [[CrossRef](#)]
59. Xu, L.H.; Liu, H.T.; Murray, B.P.; Callebaut, C.; Lee, M.S.; Hong, A.; Strickley, R.G.; Tsai, L.K.; Stray, K.M.; Wang, Y.J.; et al. Cobicistat (GS-9350): A Potent and Selective Inhibitor of Human CYP3A as a Novel Pharmacoenhancer. *Acs Med. Chem. Lett.* **2010**, *1*, 209–213. [[CrossRef](#)]
60. AIDSinfo FDA-Approved HIV Medicines. Available online: <https://aidsinfo.nih.gov/understanding-hiv-aids/fact-sheets/21/58/fda-approved-hiv-medicines> (accessed on 30 March 2020).



© 2020 by the authors. Licensee MDPI, Basel, Switzerland. This article is an open access article distributed under the terms and conditions of the Creative Commons Attribution (CC BY) license (<http://creativecommons.org/licenses/by/4.0/>).